The Effects of Strong Ageostrophic Outflows on the Formation of Surface Mesoscale Pressure Systems in Squall Lines*

JIANG Yongqiang[1,2](姜勇强) and WANG Yuan[1†](王 元)

1 *Key Laboratory of Mesoscale Severe Weather/Ministry of Education of China, and School of Atmospheric Sciences, Nanjing University, Nanjing* 210093

2 *Institute of Meteorology, PLA University of Science and Technology, Nanjing* 211101

(Received July 9, 2009; revised December 30, 2009)

ABSTRACT

Based on the previous study of the streamline field triggered by singularities in a two-dimensional potential flow, the wind field caused by vorticity lines in an incompressible flow is deduced in this paper. The result shows an elliptic cyclonic (anticyclonic) circulation in association with a positive (negative) vorticity line. By use of the shallow-water model, the flow fields are simulated in a weak wind background under the influence of mesoscale vorticity lines. In the case of two vorticity line, one positive and the other negative, a mesoscale vortex couplet forms in the flow. When three vorticity lines are considered, three mesoscale circulations develop, and a mesohigh and two mesolows similar to the thunderstorm high, wake low and pre-squall mesolow of a mature squall line are produced.

Theoretical analysis and numerical simulations show that the formation of the surface mesoscale pressure systems in squall lines may be partly attributed to the dynamical effects of the ageostrophic outflows. The strong downdrafts under the thundercloud base of the squall line lead to surface ageostrophic outflows, and produce positive-negative-positive arranged vertical vorticity bands (VBs) along the direction normal to the squall line, then the mesoscale circulations develop and mesoscale pressure systems form or strengthen during the geostrophic adjustment. By use of the scale separation method, this dynamic mechanism is confirmed by a case study of a severe storm passing over eastern China on 17 June 1974.

Key words: squall line, ageostrophic wind, vorticity line, mesoscale pressure system

Citation: Jiang Yongqiang and Wang Yuan, 2010: The effects of strong ageostrophic outflows on the formation of surface mesoscale pressure systems in squall lines. *Acta Meteor. Sinica*, **24**(2), 225–238.

1. Introduction

Squall line is one of the important mesoscale severe weather systems. The mid-latitude squall lines were studied by a number of researchers (Newton, 1950; Fujita, 1955; Pedgley, 1962; Sanders and Paine, 1975). Some other meteorologists (Hamilton and Archbold, 1945; Zipser, 1969, 1977; Houze, 1977) investigated tropical squall lines. From then on, many studies on large-scale kinematic and thermodynamic structures of squall lines were carried out (Ogura and Chen, 1977; Ogura and Liou, 1980; Gamache and Houze, 1982, 1985; Houze and Rappaport, 1984; Leary and Rappaport, 1987). However, these studies did not show much detail of the mesoscale circulation patterns of squall lines because of limited temporal and spatial resolutions of the data. With the aid of Doppler radar, mesoscale studies on squall line circulations and structures were carried out successfully (Roux et al., 1984, 1988; Smull and Houze, 1985, 1987a; Heymsfield and Schotz, 1985; Srivastava et al., 1986; Kessinger et al., 1987a, b; Chong et al., 1987). During May and June 1985, the Oklahoma-Kansas Preliminary Regional Experiment for STORM-Central (the Oklahoma-Kansas PRE-STORM Program; Cunning, 1986) was conducted to investigate the structure and dynamics of mesoscale convective systems. Several years after that, squall lines had become a hot topic in mesoscale meteorology. With regard to the squall line of 10–11 June 1985, many observations, analyses (Leary and Rappaport, 1987; Smull and Houze, 1987b; Rutledge et al., 1988; Johnson and Hamilton, 1988;

*Supported jointly by the National Fundamental Research "973" Program of China under Grant No. 2004CB418301 and the National Natural Science Foundation of China under Grant Nos. 40775034 and 40830958.

†Corresponding author: yuanasm@nju.edu.cn.

Stumpf et al., 1991; Biggerstaff and Houze, 1991a, b, 1993; Braun and Houze, 1994), and numerical simulations (Zhang et al., 1989a, b) have been performed to discuss its mesoscale structure, formation and development processes. With the use of high resolution rawinsonde, profiler, surface station, and Doppler radar data, the above studies have led to new insights into the mesoscale structure of the squall line, and greatly promoted the development of mesoscale meteorology. Later, as more and more Doppler data become available, observational studies and numerical simulations have revealed more characteristics of squall lines (Weisman and Trapp, 2003; Trapp and Weisman, 2003; Atkins and Arnott, 2004; Fovell et al., 2006; Sun and Zhang, 2008; Grim et al., 2009).

Many studies have shown that the surface pressure field of a mature squall line is characterized by a pre-squall mesolow, a mesohigh, and a wake low (Fujita, 1955; Pedgley, 1962; Schaefer et al., 1985). Fujita (1955) developed an array of techniques for the analysis of subsynoptic weather phenomena in the 1940s. His studies along with his subsequent work at the University of Chicago in the early 1950s formed the foundation of mesoscale weather system research (Johnson, 2001). Fujita mainly gave his efforts to mesohighs and wake lows. There are also different explanations for the formation of these mesoscale pressure systems of the squall line.

Some early researches attributed the genesis of the thunderstorm high to evaporation of precipitation in downdrafts (Humphreys, 1929; Suckstorff, 1935). Sawyer (1946) and Fujita et al. (1956) brought up the same viewpoint. The thunderstorm project also showed that the main reason for the formation of mesohigh is the evaporation of precipitation under the cloud base (Byers and Braham, 1949; Fujita, 1959). Fujita (1959) speculated that melting snow or hail could also contribute to the surface mesohigh, and Atlas et al. (1969) confirmed this idea. The aforementioned studies attributed the mesohigh to a hydrostatic phenomenon, which was accepted by most of researchers. However, some argued about the role of dynamical effects. When Sawyer (1946) indicated the mechanism of evaporation of precipitation in downdrafts, he also pointed out the possibility of nonhydrostatic pressure rise due to the impact of the downdrafts. Later, some studies analyzed the relative contributions of hydrostatic and nonhydrostatic pressure to the mesohigh based on tower observations, Doppler radar and sounding data (Charba, 1974; Goff, 1976; Wakimoto, 1982). After the PRE-STORM, the wind fields and pressure structures of squall lines were analyzed comprehensively by using high-resolution data. Based on the observations, the mesohigh is centered several tens of kilometers behind the leading convective line. This location suggests cumulonimbus downdrafts as a principal source for the cool mesohigh (Johnson and Hamilton, 1988).

There were many explanations for the formation of wake low. Fujita (1955) initially explained the wake depression as a dynamical response to storm-relative front-to-rear flow around the cold dome, much like the low pressure produced due to flow separation in the wake of a blunt body. However, Fujita (1963) retracted these ideas on the basis that the horizontal dimension of the mesohigh is too large to warrant the development of the wake flow, but he did not give a reasonable explanation for the formation of the wake low. Pedgley (1962) found the same characteristic surface pressure patterns reported by Fujita (1955, 1963) by analyzing a squall line passing over England on 28 August 1958. He called this mesolow as wake low. However, Pedgley either could not offer an adequate explanation for it. He suggested the explanation of Fujita (1955) as one possible reason; and the hypothesis put forward by Brunk (1953) that the tops of towering clouds may generate gravity waves on the tropopause, which would then produce pressure fluctuations at the ground as another. Koch et al. (1988) argued that the surface pressure fields in squall line systems reflected a coupling between convection and gravity waves. The computations by Williams (1963) indicated that subsidence warming might be a reason for the formation of wake low, but he could not give the reason for subsidence. Johnson and Hamilton (1988) suggested by analyzing PRE-STORM data that the wake low is a surface manifestation of the descending rear-inflow-jet and the warming is maximized at the back edge of the trailing stratiform precipitation area where there is insufficient sublimation and evaporative cooling to offset adiabatic warming. Some studies indicated that the most intense surface pressure gradients were collocated with regions where the rear-inflow jet appeared to be blocked and did not continue forward through the stratiform rain area (Stumpf et al., 1991; Johnson and Bartels, 1992; Nachamkin et al., 1994; Loehrer and Johnson, 1995), and the wake low was centered behind the intense pressure gradients. In addition, some numerical simulation studies were also performed. Wicker and Skamarock (1996) found that wake lows occur at the back edge of the cold pool where the rear-inflow jet impinges upon the trailing stratiform region. The numerical simulation conducted by Zhang and Gao (1989b) by using a three-dimensional mesoscale nested-grid model indicated that the evaporation of precipitation in the stratiform region is necessary to develop a wake low. Haertel and Johnson (2000) attributed the mesohighs and mesolows to the lower-tropospheric cooling associated with stratiform precipitation. When the moving cool source was defined to have a three-dimensional structure, both a mesohigh and a mesolow developed, having characteristics and evolutions resembling squall-line mesohighs and wake lows.

The pre-squall low (or pre-squall trough) was not specially studied by Fujita and other researchers. Hoxit et al. (1976) suggested that it may be caused by convectively induced subsidence warming in the mid- to upper troposphere ahead of squall lines. The existence of pre-squall subsidence had been confirmed by observational studies (Fankhauser, 1974; Sanders and Paine, 1975; Gamache and Houze, 1982; Gallus and Jonhnson, 1991). Numerical simulations presented by Fritsch and Chappell (1980) also confirmed the viewpoint of Hoxit et al. (1976).

Though the above studies gave a number of explanations for mesohighs and mesolows, none of these was perfect. Biggerstaff and Houze (1991a, b) analyzed the kinematics, precipitation and midlevel vorticity structure of a mature squall line. They noted that the relative vertical vorticity at midlevels of troposphere was organized into three bands oriented parallel to the convective line, with anticyclonic vorticity between the rear of the convective line and the heaviest stratiform precipitation, and one cyclonic vorticity band (VB) farther back and another in front of the convective line. Observational studies showed that there exist strong ageostrophic outflows behind the squall line, and the onward winds are usually stronger than the rearward winds. These ageostrophic outflows produce the vertical VBs along the convective line, with a positive VB in front of the squall line, a negative VB in the rear of the convective line, and another positive VB next to the negative VB. Based on the above studies, we hypothesize that the surface mesoscale pressure systems may be related to the vertical VBs. Brown (1991) deduced the streamline fields resulted from a singularity (e.g., dot vortex) by using potential flow assumptions and cylindrical coordinates. He found that in the irrotational and nondivergence flow, the Laplacian of stream function and potential function are all zero. In Section 2 of this study, a streamline field caused by vorticity lines is deduced. It indicates that the ageostrophic outflows associated with vertical VBs could trigger three mesoscale vortices which are similar to the pressure structures of the squall line. Based on the geostrophic adjustment of pressure field toward wind field in mesoscale systems, if a vortex exists in the streamline field, a corresponding high or low in pressure field may form during the geostrophic adjustment. In Section 3, a shallow-water model with a perfect initial wind field representing ageostrophic outflows is employed to simulate the formation of mesoscale vortices. In Section 4, the vorticity, wind and pressure fields of a severe storm over eastern China on 17 June 1974 are analyzed to examine the above results. Conclusions and discussion are given in the last section.

2. Flow field caused by vorticity lines

In squall line systems, when the strong downdrafts under the thundercloud base reach the ground, they will turn into strong ageostrophic winds flowing out. In this study, the outflows are divided into two parts along the squall line. One part flows toward the squall line, and the other flows rearward. The discontinuous banded outflows will produce three vertical VBs along the squall line: a negative VB near the location of the downdft, a positive VB in front of the negative VB, and another positive VB in the rear of the negative VB. These three VBs should be approximately taken as vorticity lines for their narrow widths. So there are two questions to be answered: What kind of flow field does the vorticity line cause? Is there any relationship between the triggered flow field and the mesoscale pressure distribution?

In general, the velocity of a fluid comprises two components

$$\boldsymbol{V} = \boldsymbol{V}_{\mathrm{r}} + \boldsymbol{V}_{\varphi}, \tag{1}$$

where $\boldsymbol{V}_{\mathrm{r}}$ and $\boldsymbol{V}_{\varphi}$ are wind velocities determined by vorticity and divergence, respectively. If the fluid is incompressible, $\boldsymbol{V}_{\mathrm{r}}$ satisfies

$$\boldsymbol{\zeta} = \nabla \times \boldsymbol{V}_{\mathrm{r}} \neq 0, \quad D = \nabla \cdot \boldsymbol{V}_{\mathrm{r}} = 0, \tag{2}$$

where $\boldsymbol{\zeta}$ and D is vorticity vector and divergence of the flow.

Hence, we can set a potential vector $\boldsymbol{A}_{\mathrm{r}}$ satisfying

$$\boldsymbol{V}_{\mathrm{r}} = \nabla \times \boldsymbol{A}_{\mathrm{r}}. \tag{3}$$

Therefore, the vorticity vector can be expressed as

$$\boldsymbol{\zeta} = \nabla \times \boldsymbol{V}_{\mathrm{r}} = \nabla \times \nabla \times \boldsymbol{A}_{\mathrm{r}} = \nabla(\nabla \cdot \boldsymbol{A}_{\mathrm{r}}) - \nabla^2 \boldsymbol{A}_{\mathrm{r}}, \tag{4}$$

where $\nabla \cdot \boldsymbol{A}_{\mathrm{r}}$ can be set to zero without losing universality. Otherwise, we can select a function vector $\boldsymbol{A}_1$ with $\nabla \cdot \boldsymbol{A}_1 \neq 0$, then a scalar function F can be introduced, and it satisfies

$$\boldsymbol{A}_{\mathrm{r}} = \boldsymbol{A}_1 + \nabla F.$$

Thus,

$$\boldsymbol{V}_{\mathrm{r}} = \nabla \times \boldsymbol{A}_{\mathrm{r}} = \nabla \times \boldsymbol{A}_1,$$
$$\nabla \cdot \boldsymbol{A}_{\mathrm{r}} = \nabla \cdot \boldsymbol{A}_1 + \nabla^2 F.$$

So we can select an appropriate F to satisfy $\nabla^2 F = -\nabla \cdot \boldsymbol{A}_1$. Then we also have $\nabla \cdot \boldsymbol{A}_{\mathrm{r}} = 0$. Therefore, Eq. (4) reduces to

$$\nabla^2 \boldsymbol{A}_{\mathrm{r}} = -\boldsymbol{\zeta}. \tag{5}$$

The above Poisson's equation can be integrated to obtain

$$\boldsymbol{A}_{\mathrm{r}}(x,y,z) = \frac{1}{4\pi}\int\int\int \frac{1}{r}\boldsymbol{\zeta}(X,Y,Z)\mathrm{d}X\mathrm{d}Y\mathrm{d}Z, \tag{6}$$

where (X,Y,Z) is the location of the vorticity, (x,y,z) is an arbitrary point in the space, and $r = \sqrt{(x-X)^2+(y-Y)^2+(z-Z)^2}$. Inserting Eq. (6) into Eq. (3) gives

$$\boldsymbol{V}_{\mathrm{r}} = \nabla \times \boldsymbol{A}_{\mathrm{r}}(x,y,z) = \frac{1}{4\pi}\nabla \times \int\int\int \frac{1}{r}\boldsymbol{\zeta}(X,Y,Z)\mathrm{d}X\mathrm{d}Y\mathrm{d}Z. \tag{7}$$

The x and y components of Eq. (7) are

$$u = \frac{1}{4\pi}\frac{\partial}{\partial y}\int\int\limits_{\tau}\int \frac{1}{r}\zeta_z \mathrm{d}X\mathrm{d}Y\mathrm{d}Z - \frac{1}{4\pi}\frac{\partial}{\partial z} \cdot \int\int\limits_{\tau}\int \frac{1}{r}\zeta_y \mathrm{d}X\mathrm{d}Y\mathrm{d}Z, \tag{8a}$$

$$v = -\frac{1}{4\pi}\frac{\partial}{\partial x}\int\int\limits_{\tau}\int \frac{1}{r}\zeta_z \mathrm{d}X\mathrm{d}Y\mathrm{d}Z + \frac{1}{4\pi}\frac{\partial}{\partial z} \cdot \int\int\limits_{\tau}\int \frac{1}{r}\zeta_x \mathrm{d}X\mathrm{d}Y\mathrm{d}Z, \tag{8b}$$

where u is the eastward wind component and v is the northward wind component.

In a two-dimensional flow (i.e., in an $x-y$ plane), we set the vorticity to a line as shown in Fig. 1, and

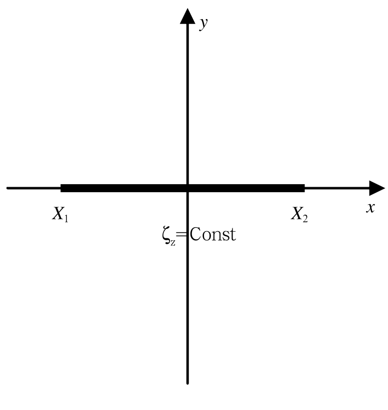

Fig. 1. The schematic diagram of a vorticity line.

the vorticity line parallel to x-axis. Hence, $\zeta_x = \zeta_y = 0$.

If $\Gamma = \int\int \zeta_z \mathrm{d}Y \mathrm{d}Z$ is taken here as a constant (i.e., all the strength of any point at the vorticity line is constant), Eqs. (8a) and (8b) can be written as follows:

$$u = \frac{\Gamma}{4\pi}\frac{\partial}{\partial y}\int_l \frac{\mathrm{d}X}{\sqrt{(x-X)^2+(y-Y)^2}}, \tag{9a}$$

$$v = -\frac{\Gamma}{4\pi}\frac{\partial}{\partial x}\int_l \frac{\mathrm{d}X}{\sqrt{(x-X)^2+(y-Y)^2}}. \tag{9b}$$

Differentiating Eqs. (9a) and (9b) gives:

$$u = -\frac{\Gamma}{4\pi}\int_l \frac{(y-Y)\mathrm{d}X}{\Big[(x-X)^2+(y-Y)^2\Big]^{\frac{3}{2}}}, \tag{10a}$$

$$v = \frac{\Gamma}{4\pi}\int_l \frac{(x-X)\mathrm{d}X}{\Big[(x-X)^2+(y-Y)^2\Big]^{\frac{3}{2}}}. \tag{10b}$$

The domain of vorticity line in x-direction is taken here as $X_1 \leqslant x \leqslant X_2$. Thus, integrating Eqs. (10a) and (10b) gives the winds

$$u = -\frac{\Gamma}{4\pi(y-Y)}\Big[\frac{x-X}{\sqrt{(x-X)^2+(y-Y)^2}}\Big]_{X_1}^{X_2}, \tag{11a}$$

$$v = \frac{\Gamma}{4\pi}\Big[\frac{1}{\sqrt{(x-X)^2+(y-Y)^2}}\Big]_{X_1}^{X_2}. \tag{11b}$$

Equations (11a) and (11b) are winds caused by the vorticity line. At the points $y = Y$, u has no meaning, and v has no meaning at either point (X_1, Y) or point (X_2, Y), so these points must be specially treated with.

The length of the vorticity line is prescribed as 200 km. The values of Γ and Y are taken as 3.0×10^{-5} $\mathrm{m^2\ s^{-1}}$ and zero respectively. The streamline fields based on Eqs. (11a) and (11b) are shown in Fig. 2. An elliptic cyclonic circulation forms in the case of a positive vorticity line, and a long and narrow vortex couplet forms in the case of two vorticity lines.

The above analysis shows that the two mesoscale positive and negative vorticity lines produce a mesoscale vortex couplet. Based on the mesoscale geostrophic adjustment of pressure field toward wind field, a corresponding mesolow and mesohigh should form. In other words, the strong ageostrophic outflows caused by strong downdrafts should produce a mesoscale pressure couplet. In the next section, this viewpoint will be verified by numerical simulations.

3. Numerical simulations

3.1 Introduction of the model

A shallow-water model was written by Gerhard Erbes in Stockholm University of Sweden. The model uses a two-dimensional flux form, and the inviscid and non-stratified approximation. It satisfies mass and momentum conversation, and the discontinuity phenomenon has been properly eliminated. The model adopts centered spatial difference scheme, leap frog temporal scheme with Asselin filter and radiation boundary condition.

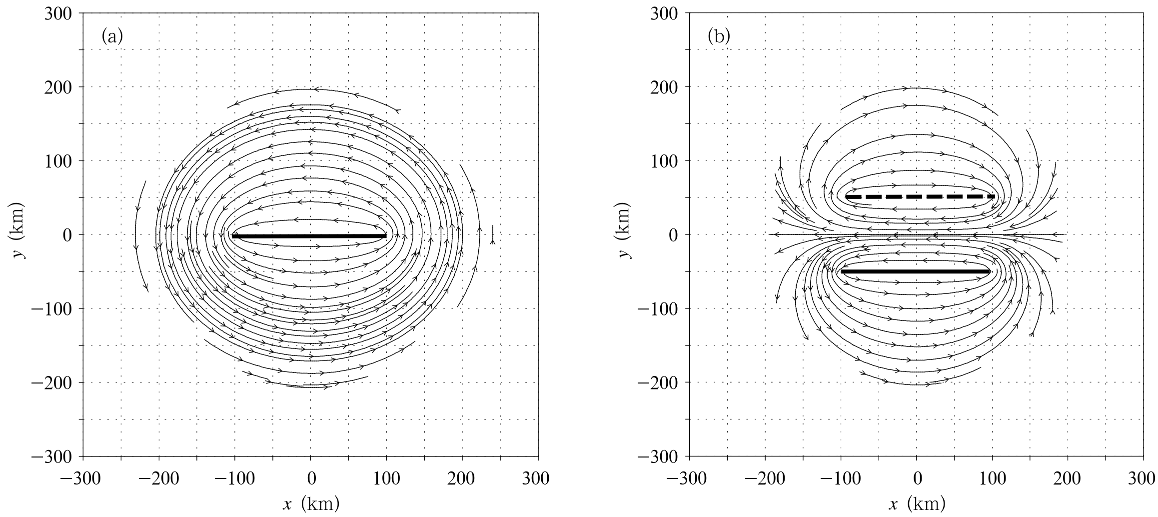

Fig. 2. (a) Streamline fields of a positive vorticity line and (b) two vorticity lines including a positive and a negative vorticity line. The heavy solid and dashed lines denote the positive and negative vorticity lines, respectively.

In Cartesian coordinates, the equations can be written as:

$$\frac{\partial(uh)}{\partial t}+\frac{\partial(u^2h+gh^2/2)}{\partial x}+\frac{\partial(vuh)}{\partial y}=s(uh),$$
$$\frac{\partial(vh)}{\partial t}+\frac{\partial(v^2h+gh^2/2)}{\partial y}+\frac{\partial(uvh)}{\partial x}=s(vh),$$
$$\frac{\partial h}{\partial t}+\frac{\partial(uh)}{\partial x}+\frac{\partial(vh)}{\partial y}=s(h),$$

where

$$s(uh)=-gh\frac{\partial h_T}{\partial x}+fvh+K\nabla^2(uh),$$
$$s(vh)=-gh\frac{\partial h_T}{\partial y}-fuh+K\nabla^2(vh),$$
$$s(h)=K\nabla^2(h),$$

where u is the eastward wind component, v the northward wind component, h the geopotential height of the free surface of the fluid, h_{T} the terrain height, K the diffusion coefficient, g the gravitational constant, f the Coriolis parameter, and ∇^2 the horizontal Laplacian operator.

The horizontal resolution of the model is 10 km. The horizontal domain of the model covers 601×601 grid elements. It is assumed that the Coriolis parameter f is a constant (the mid-latitude f-plane assumption), i.e., $f_0 = 1.26 \times 10^{-4}$ s^{-1}. The model was run for 12 h.

3.2 Background fields and banded wind perturbations

In general, the background winds are weak for squall lines. So we set the background wind to a constant westerly with the wind speed of 1 m s^{-1}. The banded wind perturbations are given as follows:

$$V'=\begin{cases} V_0 & x_1\leqslant x\leqslant x_2 \text{ and } y_1\leqslant y\leqslant y_2,\\ 0 & \text{elsewhere,}\end{cases}$$

where x_1, x_2, y_1, and y_2 are the boundary locations of the wind perturbations.

It is necessary to calculate a perturbation geopotential height h' to balance the perturbation wind. For simplicity, the constraint condition of potential vorticity (PV) conservation is used to obtain h'. The PV is defined:

$$PV=\frac{\zeta+f}{h},$$

where ζ is vertical component of the relative vorticity vector. Then

$$h'=c(\zeta'+f)=c(\frac{\partial v'}{\partial x}-\frac{\partial u'}{\partial y}+f),$$

where $c = 2.0\times10^4$. So

$$h'=\begin{cases} c(\frac{\partial v'}{\partial x}-\frac{\partial u'}{\partial y}+f), & x_1\leqslant x\leqslant x_2 \text{ and } y_1\leqslant y\leqslant y_2,\\ cf. & \text{elsewhere.}\end{cases}$$

3.3 Simulation results

3.3.1 *Two vorticity lines*

Here, the perturbations are northeasterly with V_0 of 12 m s^{-1}. The width and length of the perturbation wind field are 80 and 240 km, respectively. It represents the strong onward ageostrophic outflows in the rear of the squall line.

Figure 3a shows an initial banded northeasterly perturbation. A positive and a negative vorticity lines corresponding to positive and negative PVs form to the south and north of the perturbation wind field. Besides, there are two short vorticity lines, one to the east of the perturbation wind field and the other to the west.

Figures 3b-d show the evolution of the streamline field from $t = 1$ h to 7 h. At $t = 1$ h, cyclonic and anticyclonic circulations form at the position of positive and negative vorticity lines, respectively. This vortex couplet is similar to that of the theoretical model (Fig. 2b). However, the former has two shorter vorticity lines as described above, causing stronger local circulations. At $t = 3$ h, the center of the two circulations are stronger than before. By $t = 7$ h, the line PVs have weakened evidently. However, the PVs to the east and west of the perturbation have been organized into centers, and the circulations maintain to be west-east oriented. At the same time, another cyclonic circulation forms to the south of the perturbations.

3.3.2 *Three vorticity lines*

Considering that there are two parts of the ageostrophic outflows resulted from downdraft under the thundercloud base of the squall line, and the onward part is usually stronger than the rearward part.

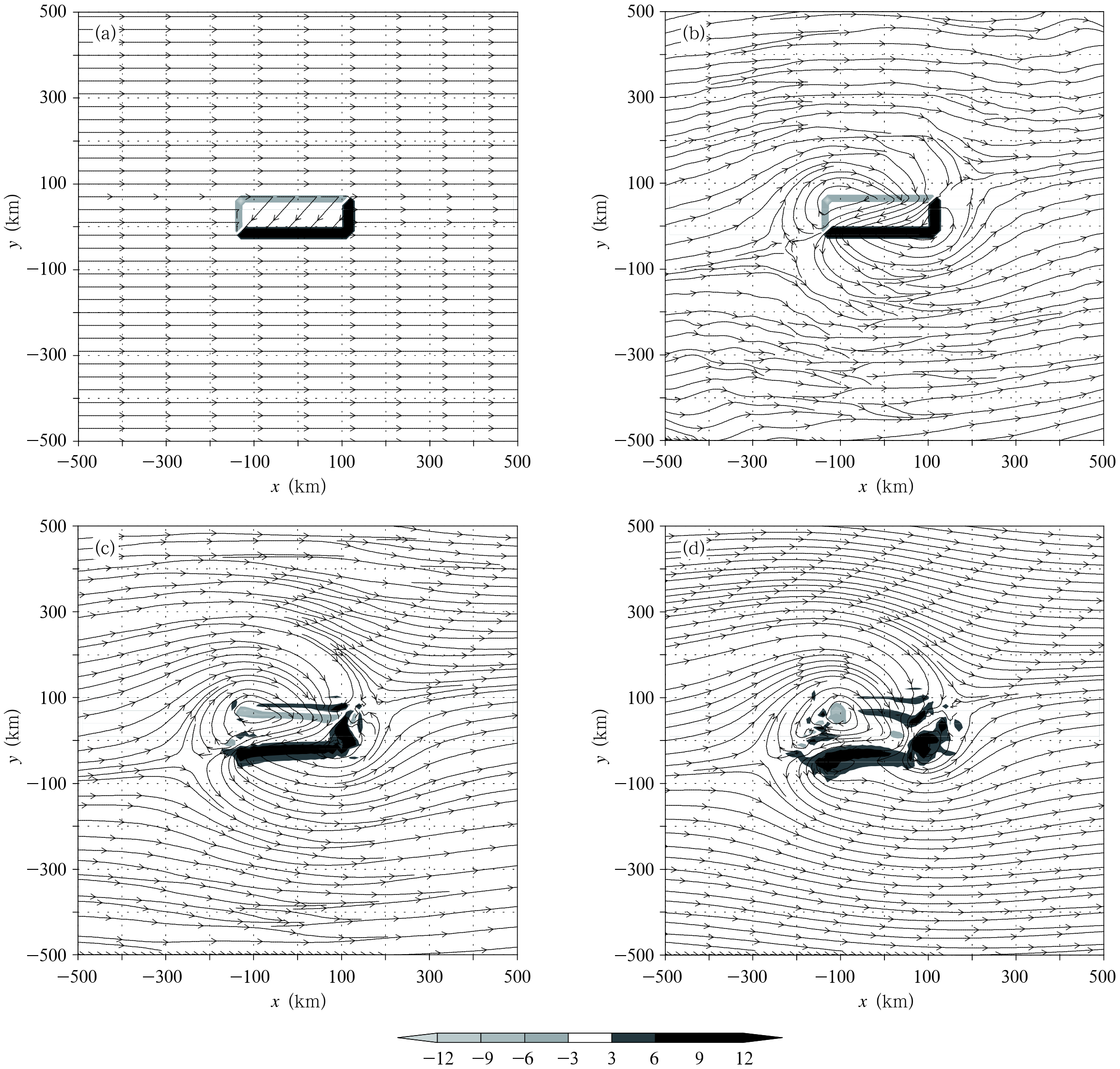

Fig. 3. Simulated streamline fields of two vorticity lines at (a) the initial time, (b) $t = 1$ h, (c) $t = 3$ h, and (d) $t = 7$ h. Shadings denote PV (10^{-8} m^{-1} s^{-1}).

Hence, besides the northeasterly perturbation with V_0 of 12 m s^{-1}, same as in the above experiment, another southwesterly perturbation with V_0 of 8 m s^{-1} is added, representing the rearward ageostrophic outflows. The width and length of perturbation wind fields are also 80 and 240 km, respectively.

The initial field is shown in Fig. 4a. The northward and southward wind perturbations produce three vorticity lines with a positive-negative-positive pattern, and the northern positive vorticity line is weaker than the southern one. At $t = 3$ h, long and narrow cyclonic and anticyclonic circulations form at the position of the southern positive and negative vorticity lines, respectively. Due to weak wind perturbations, the streamlines at the position of the northern vorticity line only form a cyclonic curve without a closed circulation. At $t = 6$ h, the southern cyclonic circulation intensifies, and a new cyclonic circulation forms to the north, though it is relative weak. At $t = 9$ h, the northern cyclonic circulation also develops into a perfect circulation, and the three circulations are all northeast-southwest oriented.

The simulated vorticity and departure of geopotential height field are shown in Fig. 5. At the beginning of integration, the geopotential height field must adjust to the wind field with the action of perturbations, and the geopotential height amplitudes change quite rapidly (figure omitted). At $t = 6$ h, corresponding to the negative vorticity line, a west-east oriented long and narrow mesohigh forms, with two center values exceeding 4 and 3 gpm, respectively. At the same time, two mesolows form corresponding to the positive vorticity lines. At $t = 12$ h, the long and narrow shaped mesohigh and mesolow are not clear. The north mesolow develops more evidently with its center value lower than −2 gpm. These three mesoscale pressure systems are similar to those of squall lines.

4. A squall line case

On 17 June 1974, a severe storm passed over eastern China. A pre-cold front warm mesolow lay over the Shandong Peninsula in mesoscale surface weather chart before 0000 UTC, and there existed a nearly west-east oriented shear line. Thereafter, a thunderstorm developed along the eastern part of the shear line, in association with a weak thunderstorm high. Then a squall line developed and moved southward. At about 0500 UTC, the squall line came to the mature stage. It had a maximum intensity at about 1200 UTC and then dissipated rapidly.

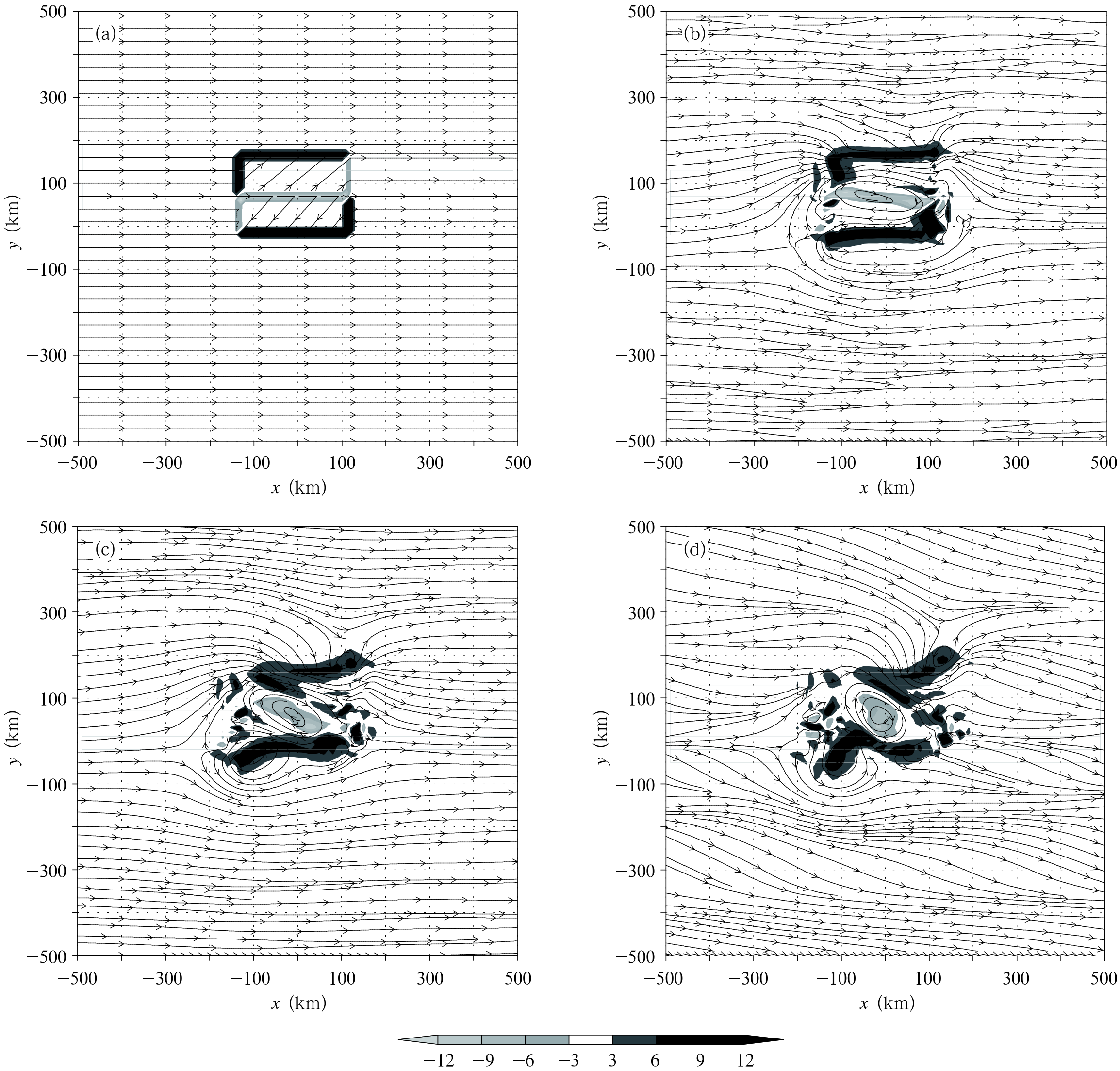

Fig. 4. Simulated streamline fields of three vorticity lines at (a) the initial time, (b) $t = 3$ h, (c) $t = 6$ h, and (d) $t = 9$ h. Others are the same as in Fig. 3.

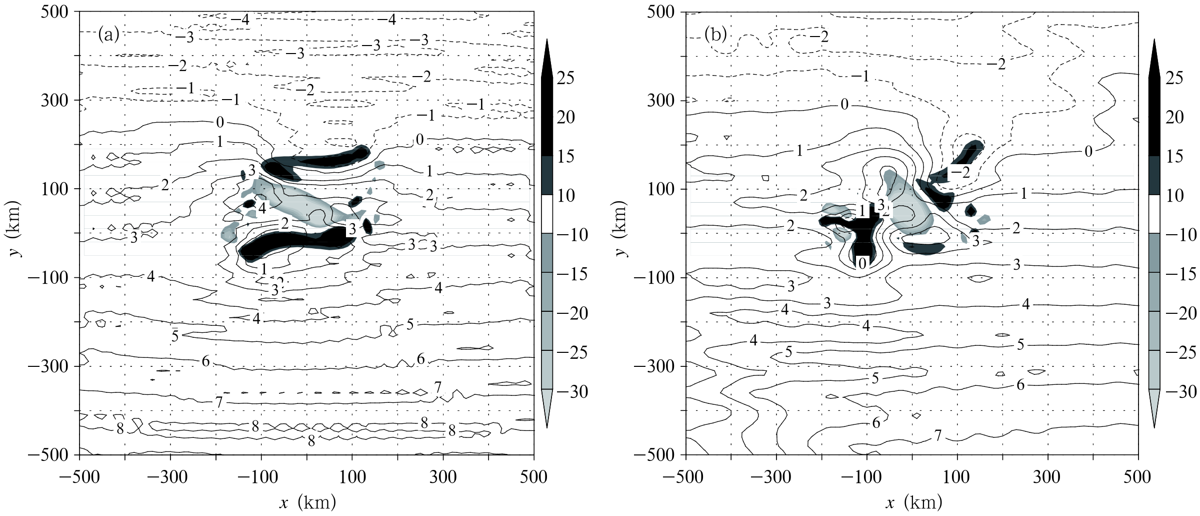

Fig. 5. Simulated vorticity field and departure of geopotential height of three vorticity lines at (a) t = 6 h and (b) t = 12 h. Shadings denote vorticity (10^{-5} s^{-1}), and lines denote the departure from mean geopotential height (= 5000 gpm).

By using observational mesoscale surface data, the grid sea level pressure (SLP), surface temperature and winds are obtained by objective analysis. Figure 6 shows the surface pattern at 0500 UTC 17 June 1974. The squall line in the pre-front warm area developed into the mature stage. There existed a quite strong mesohigh in the rear of the squall line with its center value exceeding 1002 hPa, a wake low next to the mesohigh with its center value lower than 998 hPa, and a weak pre-squall mesolow. The winds in the rear of the squall line were quite strong with wind speed exceeding 20 m s^{-1} in some areas. The winds around the mesohigh can be divided into two parts: one is onward northeasterly, with a high wind speed streak along the squall line similar to a nearly west-east oriented band, and the other is rearward southerly by the east which flows toward the wake low, with a relative weak wind speed.

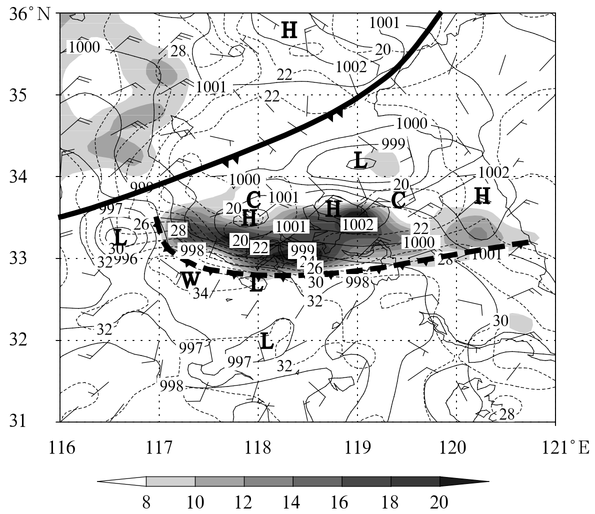

Fig. 6. The surface chart at 0500 UTC 17 June 1974. The heavy real and dashed lines with arrows denote cold front and squall line, respectively. The thin real and dashed lines denote SLP (hPa) and surface temperature (°C), respectively, and the shading denotes wind speed (m s^{-1}).

In order to analyze the mesoscale structure, the SLP, surface temperature, and wind fields are scale separated to get the large scale background and the mesoscale disturbances by use of the advanced Shuman-Shapiro filter scheme (Shapiro, 1970; Chen and Xie, 1981):

$$\begin{aligned}\overline{Z}_{i,j} = {} & Z_{i,j} + S(1-S)(Z_{i,j+1} + Z_{i,j-1} + Z_{i+1,j} \\ & + Z_{i-1,j} - 4Z_{i,j})/2 + S^2(Z_{i+1,j+1} + Z_{i+1,j-1} \\ & + Z_{i-1,j+1} + Z_{i-1,j-1} - 4Z_{i,j})/4,\end{aligned}$$

where S is the filtering coefficient. Assuming the two-dimensional wave is described as $Z = A\cos(kx + ly)$, where A is the amplitude of the wave, k and l are the x- and y-direction wave numbers, the response function can be written as

$$R = (1 - 2S\sin^2 k\Delta x/2)(1 - 2S\sin^2 l\Delta y/2).$$

By choosing appropriate values for S, we can devise response functions with suitable properties. Here, S is set as a constant of 1/2. By use of the above filter scheme and setting the space increment $\Delta x = \Delta y$, the initial field is smoothed thrice. Then the waves with wave-length less than $5\Delta x$ are attenuated by over 70%, and the waves with wave-length longer than $20\Delta x$ remain by over 95%. Here we give $\Delta x = 50$ km, and those mesoscale waves with wave-length less than 250 km will be mostly eliminated.

Figure 7 shows the scale separated large scale and mesoscale surface patterns. There are easterly flows in most areas in association with an inverted pressure trough in the large scale field. In the mesoscale field, all the mesohighs and the pre-squall mesolows have several centers, like west-east oriented bands, and the wake low located in the rear of the mesohigh is very strong. There exists a boundary close to the ridge of the mesohigh (i.e., the thick dashed line shown in Fig. 7b) along which the onward wind speed is stronger than the rearward wind speed.

Figure 8 illustrates the scale separated mesoscale SLP, streamline and vorticity distributions. Corresponding to the surface mesohighs and pre-squall mesolows, there exist band-like negative vorticity (red dashed line) and positive vorticity (blue dashed line in the south) zones with several centers lining up from west to east. The positive vorticity zone is very strong with a center value over 35×10^{-5} s^{-1}. The northern vorticity zone near the wake low is relative weak. These positive and negative vorticity zones are likely corresponding to cyclonic circulation (or cyclonic shear) and anticyclonic circulation (or anticyclonic shear), respectively. This structure is also similar to the patterns simulated in subsection 3.3.2 (see Fig. 4). However, a distinction is very clear between the simulated and the observed streamline fields. In the simulated field, there exists an anticyclonic circulation corresponding to the negative vorticity line, but in the observed field, anticyclonic shears or diffluent lines occupy the most negative vorticity area without any closed anticyclonic circulation. In the region of the observed wake low, the cyclonic circulation is not as clear as in the simulated field. On the whole, the simulated patterns are similar to the observation.

5. Conclusions and discussion

The flow fields caused by vorticity lines in an incompressible flow are deduced. There are elliptic cyclonic and anticyclonic circulations corresponding to positive and negative vorticity lines. A shallow-water model is employed to simulate the flow field caused by banded wind perturbations similar to the ageostrophic outflows. When the onward and rearward outflows are both considered, the outflows produce three vorticity

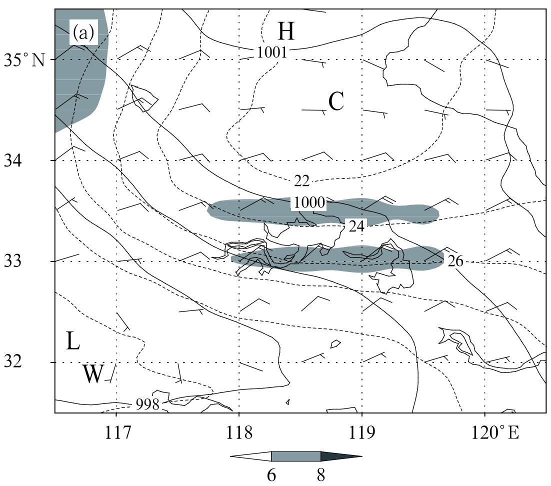

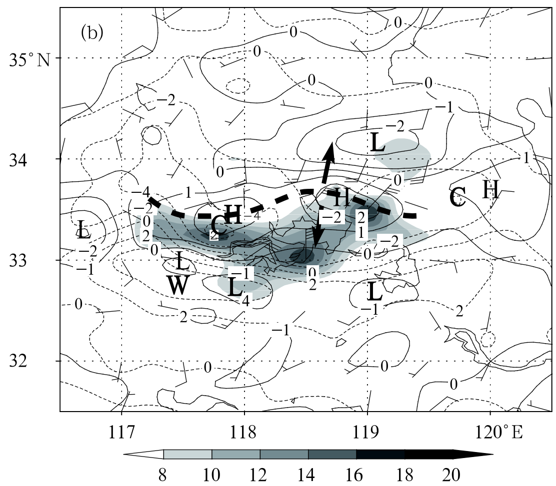

Fig. 7. Scale separated (a) large scale and (b) mesoscale surface charts at 0500 UTC 17 June 1974. The real line represents SLP (hPa), and the thin dashed line surface temperature (°C). The thick dashed line is the boundary between southward and northward outflows. Shadings denote the wind speed (m s^{-1}), and the thick arrows denote the outflows.

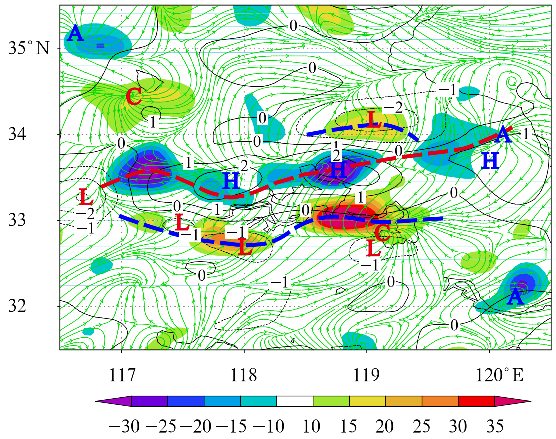

Fig. 8. Scale separated mesoscale pressure, streamline and vorticity fields at 0500 UTC 17 June 1974. Black lines represent SLP (hPa), green arrow lines are streamlines, shadings denote vorticity (10^{-5} s^{-1}), and blue and red dashed lines denote positive and negative vorticity, respectively.

lines and then trigger three mesoscale circulations. A mesohigh and two mesolows are also simulated corresponding to negative and positive vorticity lines. These three mesoscale vortices are similar to the thunderstorm high, wake low, and pre-squall mesolow of the mature squall line.

The vorticity, streamline, and SLP fields are analyzed for a mature severe storm passing over eastern China on 17 June 1974. The large scale and mesoscale SLP, temperature and wind fields are obtained by use of the scale separation method. In the mesoscale wind field, there are southward (or onward) and northward (or rearward) outflows around the mesohigh. The wind speed of onward outflows is stronger than that of rearward outflows. The mesoscale vorticity field exhibits three VBs near the mesohighs and mesolows.

The numerical simulation results show that certain mesoscale circulations form at the position of VBs after some time of integration with the action of banded wind perturbations. It indicates that when the strong downdrfts under the thunder cloud bring about the banded outflows, the mesoscale outflows could produce positive and negative VBs, and the mesoscale circulations then develop during the geostrophic adjustment. Because the pressure field adjusts to wind field in the mesoscale setting, the mesohighs and mesolows may form. In fact, there usually exist two parts of the outflow associated with three VBs. Thus, some pressure structures similar to mesohigh, pre-squall mesolow and wake low form.

Based on Fujita (1963), a squall mesosystem develops as a small mesohigh and dissipates as a mesodepression after going through five stages. At the initiation stages, a small mesohigh which can be detected only by a (meso) network forms and develops, and during the development and mature stages, a wake low develops behind the mesohighs. But the formation process of the pre-squall mesolow was not given in that study. According to Fujita's idea, the mesohighs which first form must be accompanied by strong downdrafts associated with strong ageostrophic outflows on the ground. The VBs produced by ageostrophic outflows then strengthen the corresponding mesohighs and mesolows. This dynamical mechanism exists all the time during the development of the squall line, and it can partly explain the formation of wake low and pre-squall mesolow. However, the rearward outflows as well as the simulated wake low are usually relatively weak, which disagrees with observational facts that the wake low is usually strong. So the above dynamical explanation for the wake low may be lack of soundness. Certainly, if the rearward outflows are strong enough, the wake low must be rather strong. As to the pre-squall mesolow, Hoxit et al. (1976) attributed it to convectively induced subsidence warming in the mid- to upper troposphere ahead of squall lines. The formative mechanism of mesoscale pressure systems proposed in this study may serve as another explanation.

REFERENCES

Atlas, D., R. Tatehira, R. C. Srivastava, et al., 1969: Precipitation-induced mesoscale wind perturbations in the melting layer. *Quart. J. Roy. Meteor. Soc.*, **95**, 544–560.

Atkins, N. T., and J. M. Arnott, 2004: Vortex structure and evolution within bow echoes. Part I: Single-doppler and damage analysis of the 29 June 1998 Derecho. *Mon. Wea. Rev.*, **132**, 2224–2242.

Biggerstaff, M. I., and R. A. Houze Jr., 1991a: Kinematic and precipitation structure of the 10–11 June 1985 squall line. *Mon. Wea. Rev.*, **119**, 3034–3065.

——, and ——, 1991b: Midlevel vorticity structure of the 10-11 June 1985 squall line. *Mon. Wea. Rev.*, **119**, 3066–3079.

——, and ——, 1993: Kinematics and microphysics of the transition zone of the 10–11 June 1985 squall line. *J. Atmos. Sci.*, **50**, 3091–3110.

Braun, S. A., and R. A. Houze Jr., 1994: The transition zone and secondary maximum of radar reflectivity behind a midlatitude squall line: Results retrieved from Doppler radar data. *J. Atmos. Sci.*, **51**, 2733–2755.

Brown, R. A. 1991: *Fluid Mechanics of the Atmosphere.* Academic Press, INC. 489 pp.

Brunk, I. W., 1953: Squall lines. *Bull. Amer. Meteor. Soc.*, **34**, 1–9.

Byers, H. R., and R. R. Braham Jr., 1949: The thunderstorm. U. S. Government Printing Offices, Washington, DC, 287 pp.

Charba, J. 1974: Application of gravity current model to analysis of squall-line gust front. *Mon. Wea. Rev.*, **102**, 140–156.

Chen Shoujun and Xie An, 1981: Diagnostic analysis on the exchange of kinetic energy between subsynoptic scale and synoptic scale weather systems. *Acta Meteor. Sinica*, **39**(4), 408–415. (in Chinese).

Chong, M., P. Amayenc, G. Scialom, et al., 1987: A tropical squall line observed during the COPT 81 experiment in West Africa. Part I: Kinematic structure inferred from dual-Doppler radar data. *Mon. Wea. Rev.*, **115**, 670–694.

Cunning, J. B., 1986: The Oklahoma-Kansas preliminary regional experiment for STORM-Central. *Bull. Amer. Meteor. Soc.*, **67**, 1478–1486.

Fankhouser, J. C., 1974: The derivation of consistent fields of wind and geopotential height from mesoscale rawinsonde data. *J. Appl. Meteor.*, **13**, 637–646.

Fovell, R. G., G. L. Mullendore, and S. H. Kim, 2006: Discrete propagation in numerically simulated nocturnal squall lines. *Mon. Wea. Rev.*, **134**, 3735–3752.

Fritsch, J. M., and C. F. Chappell, 1980: Numerical prediction of convectively driven mesoscale pressure systems. Part II: Mesoscale model. *J. Atmos. Sci.*, **37**, 1734–1762.

Fujita, T. T., 1955: Results of detailed synoptic studies of squall lines. *Tellus*, **7**, 405–436.

——, 1959: Precipitation and cold air production in mesoscale thunderstorm systems. *J. Meteor.*, **16**, 454–466.

——, 1963: Analytical mesometeorology: A review. Meteorological Monograph, 5, No. 27, Amer. Meteor. Soc., 77–125.

——, H. Newstein, and M. Tepper, 1956: Mesoanalysis-An important scale in the analysis of weather data. U. S. Weather Bureau Research Res. Paper 39, Washington, DC, 83 pp.

Gallus, W. A. Jr., and R. H. Johnson, 1991: Heat and moisture budgets of an intense midlatitude squall line. *J. Atmos. Sci.*, **48**, 122–146.

Gamache, J. F., and R. A. Houze Jr., 1982: Mesoscale air motions associated with a tropical squall line. *Mon. Wea. Rev.*, **110**, 118–135.

——, and ——, 1985: Further analysis of the composite wind and thermodynamic structure of the 12 September GATE squall line. *Mon. Wea. Rev.*, **113**, 1241–1259.

Goff, C. R., 1976: Vertical structure of thunderstorm outflows. *Mon. Wea. Rev.*, **104**, 1429–1440.

Grim, J. A., R. M. Rauber, G. M. McFarquhar, et al., 2009: Development and forcing of the rear inflow jet in a rapidly developing and decaying squall line during BAMEX. *Mon. Wea. Rev.*, **137**, 1206–1229.

Haertel, P. T., and R. H. Johnson, 2000: The linear dynamics of squall line mesohighs and wake lows. *J. Atmos. Sci.*, **57**, 93–107.

Hamilton, R. A., and J. W. Archbold, 1945: Meteorology of Nigeria and adjacent territory. *Quart. J. Roy. Meteor. Soc.*, **83**, 303–314.

Heymsfield, G. M., and S. Schotz, 1985: Structure and evolution of a severe squall line over Oklahoma. *Mon. Wea. Rev.*, **113**, 1563–1589.

Houze, R. A. Jr., 1977: Structure and dynamics of a tropical squall-line system. *Mon. Wea. Rev.*, **105**, 1540–1567.

——, and E. N. Rappaport, 1984: Air motions and precipitation structure of an early summer squall line over the eastern tropical Atlantic. *J. Atmos. Sci.*, **41**, 553–574.

Hoxit, L. R., C. F. Chappell, and J. M. Fritsch, 1976: Formation of mesolows or pressure troughs in advance of cumulonimbus clouds. *Mon. Wea. Rev.*, **104**, 1419–1428.

Humphreys, W. J., 1929: *Physics of the Air.* McGraw-Hill, 654 pp.

Johnson, R. H., and P. J. Hamilton, 1988: The relationship of surface pressure features to the precipitation and airflow structure of an intense midlatitude squall line. *Mon. Wea. Rev.*, **116**, 1444–1473.

——, and D. L. Bartels, 1992: Circulations associated with a mature-to-decaying midlatitude mesoscale convective system. Part II: Upper-level features. *Mon. Wea. Rev.*, **120**, 1301–1320.

——, 2001: Surface mesohighs and mesolows. *Bull. Amer. Meteor. Soc.*, **82**, 13–31.

Kessinger, C. J., P. S. Ray, and C. E. Hane, 1987a: The Oklahoma squall line of 19 May 1977. Part I: A multiple Doppler analysis of convective and stratiform structure. *J. Atmos. Sci.*, **44**, 2840–2864.

——, ——, and ——, 1987b: The Oklahoma squall line of 19 May 1977. Part II: Mechanisms for maintenance of the region of strong convection. *J. Atmos. Sci.*, **44**, 2866–2883.

Koch, S. E., R. E. Golus, and P. B. Dorian, 1988: A mesoscale gravity wave event observed during CCOPE. Part II: Interactions between mesoscale convective systems and antecedent waves. *Mon. Wea. Rev.*, **116**, 2545–2569.

Leary, C. A., and E. N. Rappaport, 1987: The life cycle and internal structure of a mesoscale convective complex. *Mon. Wea. Rev.*, **115**, 1503–1527.

Loehrer, S. M., and R. H. Johnson, 1995: Surface pressure and precipitation life cycle characteristics of PRE-STORM mesoscale convective systems. *Mon. Wea. Rev.*, **123**, 600–621.

Nachamkin, J. E., R. L. McAnelly, and W. R. Cotton, 1994: An observational analysis of a developing mesoscale convective complex. *Mon. Wea. Rev.*, **122**, 1168–1188.

Newton, C. W., 1950: Structure and mechanisms of the prefrontal squall. *J. Meteor.*, **7**, 210–222.

Ogura, Y., and Y. L. Chen, 1977: A life history of an intense mesoscale convective storm in Oklahoma. *J. Atmos. Sci.*, **34**, 1458–1476.

——, and M. T. Liou, 1980: The structure of a midlatitude squall line: A case study. *J. Atmos. Sci.*, **37**, 553–567.

Pedgley, D. E., 1962: A meso-synoptic analysis of the thunderstorms on 28 August 1958. Geophysical Memo., 106, British. Meteor. Office, 74 pp.

Roux, F., 1988: The west African squall line observed on 23 June 1981 during COPT 81: Kinematics and thermodynamics of the convective region. *J. Atmos. Sci.*, **45**, 406–426.

——, J. Testud, M. Payen, et al., 1984: West African squall-line thermodynamic structure retrieved from dual-Doppler radar observations. *J. Atmos. Sci.*, **41**, 3104–3121.

Rutledge, S. A., R. A. Houze Jr., M. I. Biggerstaff, et al., 1988: The Oklahoma-Kansas mesoscale convective system of 10–11 June 1985: Precipitation structure and single-Doppler radar analysis. *Mon. Wea. Rev.*, **116**, 1409–1430.

Sanders, F., and R. J. Paine, 1975: The structure and thermodynamics of an intense storm in Oklahoma. *J. Atmos. Sci.*, **32**, 1563–1579.

Sawyer, J. S., 1946: Cooling by rain as a cause of the pressure rise in convectional squalls. *Quart. J. Roy. Meteor. Soc.*, **72**, 168.

Schaefer, J. T., L. R. Hoxit and C. F. Chappell, 1985: Thunderstorms and their mesoscale environment. Thunderstorm Morphology and Dynamics, Edwin Kessler, Ed., University of Oklahoma Press, 113–130.

Shapiro, R., 1970: Smoothing, filtering, and boundary effects. *Rev. Geophys. Space Phys.*, **8**, 359–387.

Smull, B. F., and R. A. Houze Jr., 1985: A mid-latitude squall line with a trailing region of stratiform rain radar and satellite observations. *Mon. Wea. Rev.*, **113**, 117–133.

——, and ——, 1987a: Dual-Doppler radar analysis of a midlatitude squall line with a trailing region of stratiform rain. *J. Atmos. Sci.*, **44**, 2128–2148.

——, and ——, 1987b: Rear inflow in squall lines with trailing stratiform precipitation. *Mon. Wea. Rev.*, **115**, 2869–2889.

Stumpf, G. J., R. H. Johnson, and B. F. Smull, 1991: The wake low in a midlatitude mesoscale convective system having complex convective organization. *Mon. Wea. Rev.*, **119**, 134–158.

Srivastava, R. C., T. J. Matejka, and T. J. Lorello, 1986: Doppler radar study of the trailing anvil region associated with a squall line. *J. Atmos. Sci.*, **43**, 356–377.

Suckstorff, G. A., 1935: Die strömmungsvorgänge in instabilitätschauern. *Z. Meteor.*, **25**, 449–452.

Sun, J. Z., and Y. Zhang, 2008: Analysis and prediction of a squall line observed during IHOP using multiple WSR-88D observations. *Mon. Wea. Rev.*, **136**, 2364–2388.

Trapp, R. J., and M. L. Weisman, 2003: Low-level mesovortices within squall lines and bow echoes. Part II: Their genesis and implications. *Mon. Wea. Rev.*, **131**, 2804–2823.

Wakimoto, R. M., 1982: Life cycle of thunderstorm gust fronts as viewed with Doppler radar and rawinsonde data. *Mon. Wea. Rev.*, **110**, 1060–1082.

Weisman, M. L., and R. J. Trapp, 2003: Low-level mesovortices within squall lines and bow echoes. Part I: Overview and dependence on environmental shear. *Mon. Wea. Rev.*, **131**, 2779–2803.

Wicker, L. J., and W. C. Skamarock, 1996: The dynamics governing surface pressure fields in mesoscale convective systems. Preprints, Seventh Conf. on Mesoscale Processes, Reading, United Kingdom, Amer. Meteor. Soc., 476–478.

Williams, D. T., 1963: The thunderstorm wake of May 4, 1961. Nat. Severe Storms Project Rep. 18, U. S. Dept. of Commerce, Washington, DC, 23 pp. [NTIS PB-168223].

Zhang, D. L., K. Gao, and D. B. Parsons, 1989a: Numerical simulation of an intense squall line during 10–11 June 1985 PRE-STORM. Part I: Model verification. *Mon. Wea. Rev.*, **117**, 960–994.

——, and ——, 1989b: Numerical simulation of an intense squall line during 10–11 June 1985 PRE-STORM. Part II: Rear inflow, surface pressure perturbations and stratiform precipitation. *Mon. Wea. Rev.*, **117**, 2067–2094.

Zipser, E. J., 1969: The role of organized unsaturated convective downdrafts in the structure and rapid decay of an equatorial disturbance. *J. Appl. Meteor.*, **8**, 799–814.

——, 1977: Mesoscale and convective-scale downdrafts as distinct components of squall-line structure. *Mon. Wea. Rev.*, **105**, 1568–1589.